A&A 561, A24 (2014)
DOI: 10.1051/0004-6361/201322604

Astronomy & Astrophysics

Interstellar polarization at high galactic latitudes from distant stars

VIII. Patterns related to the local dust and gas shells from observations of ~3600 stars⋆

A. Berdyugin[1], V. Piirola[1], and P. Teerikorpi[2]

[1] FINCA, University of Turku, Vaisalantie 20, 21500 Piikkio, Finland
e-mail: [andber;piirola]@utu.fi
[2] Department of Physics and Astronomy, University of Turku, Vaisalantie 20, 21500 Piikkio, Finland
e-mail: pekkatee@utu.fi

Received 4 September 2013 / Accepted 21 November 2013

ABSTRACT

Aims. Interstellar polarization of starlight at high galactic latitudes gives information on the direction of the local Galactic magnetic field and the distribution of cosmic dust in wide "windows" perpendicular to the Galactic plane. Polarization data allow us to construct for the first time high-latitude polarization maps with resolution and sky coverage high enough to examine in detail the distribution of the interstellar polarization and the direction of the Galactic magnetic field around Galactic poles.
Methods. We measured the polarization for more than 2400 new stars at distances of up to 600 pc and within 60° and 30° from the north and south Galactic poles. Here we describe the measurements and properties of the resulting total sample of about 3600 stars (completeness, radial distribution), and present polarization maps of the regions around the north ($b > 30°$) and south ($b > 60°$) poles.
Results. The new interstellar polarization maps give wider and higher resolution views around the Galactic poles than previous maps. The major patterns in the maps are significant asymmetries in the polarization, one in the northern sky directly across the local spiral and the second between the northern and southern Galactic hemispheres. We confirm that there is significantly more interstellar polarization at high southern latitudes than at high northern latitudes within the local spiral. A comparison of our optical polarization map with the proposed models using local dust- and gas shells, (i.e., Weaver's Loop I superbubble, Wolleben's two-bubble model, the interaction between the Local Bubble and the Loop I superbubble) reveals interesting features. 1) The optical and radio polarizations are lower in the eastern than in the western branch of Loop I, which may be caused by a weaker effective magnetic field in the eastern part where the diffuse IRAS emission is bright; this illustrates that low optical polarization does not always imply little dust. 2) We can see a clear signature of the western side of Wolleben's S2 shell (at $35 < l < 55$), while there is no alignment of the polarization directions along the suggested wall of S2 in the eastern part, though the alignment along S1 is visible. 3) In the upper parts of the suggested interaction zone between the Local Bubble and the Loop I superbubble our data show polarizations aligned along the zone contour. The week and rather randomly directed polarizations measured previously in the eastern part of this region may reflect the shorter distances (<250 pc) in the investigated sample of stars.

Key words. polarization – dust, extinction – ISM: magnetic fields – local insterstellar matter – solar neighborhood

1. Introduction

In the present paper we continue our study of dust, extinction, and the geometry of the magnetic field at high northern and southern galactic latitudes from polarimetry of distant stars. We now have a unique large sample of ~3600 stars, ~2400 of which are from new observations made during 2004−2012.

The pioneering study of interstellar polarization in the areas of the north (NGP) and the south (SGP) Galactic poles was made by Appenzeller (1968). He also obtained first estimates for the interstellar reddening in these areas of the sky from the polarization measurements: $E(B-V) > 0.011$ for the NGP and $E(B-V) > 0.016$ for the SGP (Appenzeller 1975). Later, Markkanen (1979) has identified the first polarization structure at high galactic latitudes, a "dust cloud" near the NGP in the longitude range $250° < l < 40°$. The interstellar polarization near the SGP and at high southern galactic latitudes was observed by Shroder (1976) and Korhonen & Reiz (1986). Several hundreds of stars at $|b| > 30°$ were measured by Mathewson & Ford (1970) for their all-sky interstellar polarization map.

Most of the polarization measurements made at high galactic latitudes in the past have been restricted to bright and nearby stars ($d < 200$ pc). In the beginning of the 1990s, we started our program of a systematic study of the interstellar polarization at high galactic latitudes by extending observations toward larger distances and expanding the mapped area from the polar areas toward lower latitudes. The results of those observations were published in seven papers. Up to 2004, we have obtained a complete polarization map for southern latitudes $-90° < b < -70°$ and have extended the mapped area from the NGP down to $b = 60°$ (see Berdyugin & Teerikorpi 2002; Berdyugin et al. 2004, and references therein). Our studies have proved without doubt the presence of substantial amounts of dust at high galactic latitudes and have shown that the distribution of high-latitude dust is strongly nonuniform. Observations of interstellar polarization in this area of the sky clearly give a wealth of information

⋆ Table 1 with positions and polarization results is only available at the CDS via anonymous ftp to
cdsarc.u-strasbg.fr (130.79.128.5) or via
http://cdsarc.u-strasbg.fr/viz-bin/qcat?J/A+A/561/A24

on our local Galactic environment (e.g., independent estimates of the extinction and directions of the local Galactic magnetic field).

To examine more fully the polarization picture, its patterns, and its connections with the local dust- and gas shells and the local spiral arm, we decided to extend our measurements farther from the poles. During the years 2004−2012, observations of 2188 new stars in the NGP area and 218 stars in the SGP area were carried out, whose distances are available from the Hipparcos catalog. This allowed us to build a complete polarization map for high northern galactic latitudes down to $b = 30°$ and extend the mapped area around the SGP down to the $b = -60°$.

2. New observations in 2004–2012

Most of our new observations were carried out in 2004−2010 with the DiPol polarimeter (Piirola et al. 2005) installed on the remote-controlled 60 cm KVA telescope at La Palma, (Canary Islands, Spain). Because the direction of interstellar polarization only shows a week dependence on the wavelength, our observations with the DiPol were obtained in white (unfiltered) light to collect as many photons as possible. For each star we typically made 4−8 measurements of the Stokes parameters Q and U with the exposure time varying from 2 to 10 s, depending on the brightness of the star.

In November 2011, the new DiPol-2 polarimeter built at FINCA, at the University of Turku has replaced the first version of the DiPol. The new instrument uses two dichroic color-sensitive beam-splitters to simultaneously measure polarization in the B, V, and R bands. Three CCDs, Apogee Alta U47 for the B band and SBIG ST-402ME for the V, and R bands are communicating with the PC via a USB2 interface; the read-out time is ∼1 s for each CCD and the peak quantum efficiency is ≥90%. A super-achromatic $\lambda/2$ or $\lambda/4$ retarder rotated by a stepper motor is used as a polarization modulator. A calcite analyzer separates the two orthogonally polarized light beams by 1 mm in the telescope focal plane. A detailed description of the polarimeter will be given elsewhere (Piirola et al., in prep.). About 150 stars have been observed with this instrument in 2011−2012. Data obtained in the V band have been selected for the new polarization map, because for this pass-band the ratio of P/σ_P is usually highest in the case of interstellar polarization.

To calibrate of the polarization angle zero-points we observed the highly polarized standard stars HD 25443, HD 161065, and HD 204827. To estimate the value of the instrumental polarization, more than 30 nearby (<20 pc) zero-polarized stars were observed. The most precise measurements made in 2011−2012 with the DiPol-2 show that the instrumental polarization in all pass-bands is well below 0.01% (Piirola et al., in prep.), and thus negligible for this program.

Particular care was taken to avoid variable and peculiar stars that might possess intrinsic polarization. These stars were excluded from our sample. Our resulting polarization maps include only stars whose polarization was measured with a relative accuracy $P/\sigma_P > 2$. We took a star to be unpolarized ($P = 0.00\%$) if both P and $\sigma_P < 0.05\%$ and $P/\sigma_P < 1.44$. Our new measurements are given in Table 1.

3. Properties of the new data sample

Our polarization data for the area of $70° < b < 90°$ have been previously published by Berdyugin et al. (2001) and Berdyugin & Teerikorpi (2002). Here we describe only the new data for the northern galactic latitudes, collected in the area $30° < b < 70°$. The total number of stars in the new sample, used to make the polarization maps here, is about 2400. Together with the older data, there are about 3000 stars in the northern latitudes, and 660 stars in the southern latitudes. The average numbers of stars per square degree is about 0.17 and 0.15 for the northern and southern latitudes, respectively. This space density is clearly high enough to reveal large-scale polarization structures in the studied areas. The northern part of the sky in the latitude range $30° < b < 90°$ is now fully covered by our measurements. In the southern part, there are no data for the latitudes $b > -60°$ in the whole longitude range and for the latitudes $b > -70°$ in the longitude range $315° < l < 15°$. The latter part of the southern sky is not accessible from La Palma.

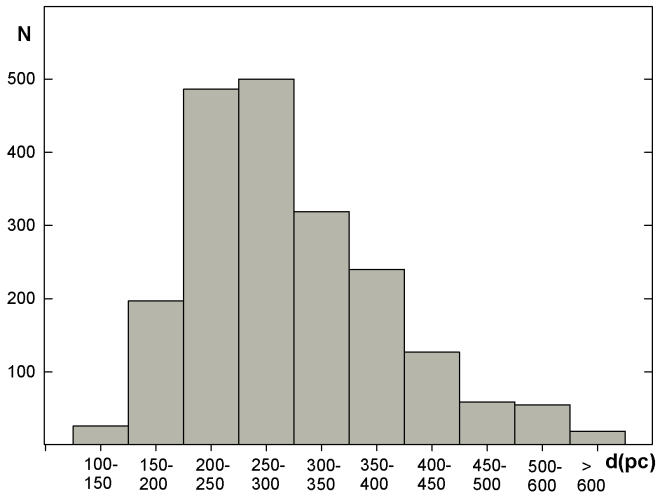

Fig. 1. Distribution of the distances of the new sample of stars observed in the latitude range $30° < b < 70°$.

Here we do not discuss the statistical properties of the southern sample, because more data are needed for this area of sky for a detailed analysis.

Figure 1 shows the distribution of the distances (as inferred from the Hipparcos parallaxes) for the newly observed stars at the northern galactic latitudes. As can be seen from Fig. 1, more than 70% of the stars in our sample are located in the distance range 200−400 pc. Therefore, our polarization study has effectively mapped the distribution of dust and the directions of the Galactic magnetic field up to the distance of 400 pc at least. The picture beyond this distance is far from being complete, and the major reason for this is the low relative precision of the Hipparcos parallaxes for stars more distant than 400 pc. For our sample we selected only stars whose accuracy in the parallax determination is better than 50%.

The distributions of the polarization values is shown in Fig. 2. A significant fraction of our sample (≈500 stars, or ≈20%) show very low or zero polarization. Most of these stars are located in the longitude range $240° < l < 60°$. However, the majority of stars (more than 60%) show a low, but substantial polarization value in the range of 0.05−0.50%. There are also many stars (≈200) with high polarizations, up to values exceeding 1%.

4. Northern circumpolar polarization map

We present the northern polarization maps in two projections, with the galactic longitude and latitude (l, b) either as rectangular

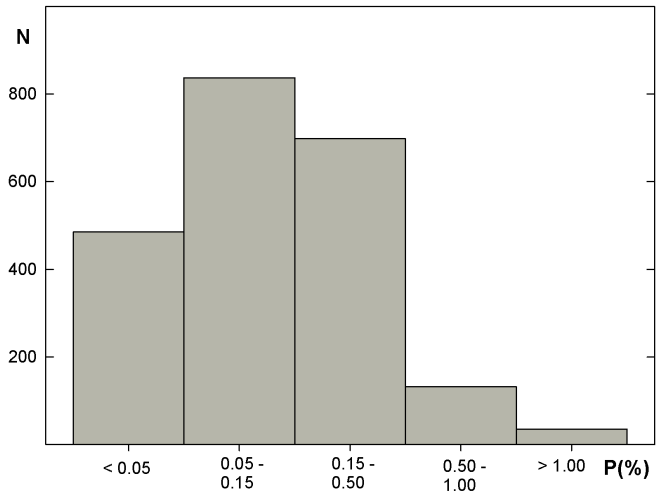

Fig. 2. Distribution of the polarizations of the new sample.

or as polar coordinates. Figure 3 shows the rectangular view: the top part is for the longitude range from 60° to 0° and 240°, and the bottom part displays the range from 240° to 60° (covering roughly the local spiral arm where the Sun is near the inner edge). The amount of polarization $P(\%)$ and its direction (the projection of the polarization vector on the sky) as measured for each star is indicated by a short line with size proportional to the polarization percentage (or by a point, if $P = 0.0$). The map also includes older data (≈300 stars) from Mathewson & Ford (1970) and Korhonen & Reiz (1986), provided that they satisfy our accuracy criterium.

Remarkable in Fig. 3 is the large difference between the appearances of the polarized sky in the two areas. In the bottom frame the interstellar polarizations are quite low (typically <0.2%) and there is hardly any directional pattern visible. A striking contrast to this monotonic view, the upper frame shows significantly higher (up to 2.0%) polarizations and regular alignments forming a coherent picture of magnetic field lines.

The most remarkable feature is a giant arch or loop between longitudes 255° and 45° with the center at longitude $l = 330°$. We clearly see the upper part of the structure in all its grandeur, which Mathewson & Ford (1970) found in their first all-sky interstellar polarization map which was based mostly on data obtained for lower latitudes and nearby stars. Although this loop was also observed in previous polarization maps, for instance, Ellis & Axon (1978), our new data reveal it with unprecedented clarity and detail.

There is another remarkable asymmetry in the magnitude of the interstellar polarizations, appearing in the loop itself: the polarizations in the western branch ($0° < l < 45°$) are much higher than in the eastern branch ($255° < l < 300°$). This difference can also be seen in Fig. 4, which shows the dependence of the polarization on the distance in three adjacent longitude zones.

Figure 4 shows much scatter in the dependence of the polarization on distance in the western and central parts of the loop: in the distance range 150 pc $< d <$ 400 pc, the polarization takes all possible values between 0.0 and 1.5−2.0%. Because in these regions the polarization directions appear to be very well aligned, this scatter can probably be explained with the patchy dust distribution in these directions up to ≈500 pc: denser clouds and empty voids are closely adjoined.

Figure 5 shows the NGP polarization map in polar coordinates. As an aid for orientation, we included a curve indicating the expected rough position of the inner edge of the local spiral feature (or the Orion spur between the Perseus and the Sagittarius arms), as suggested by spiral tracers (the NGP is within the spur: see Berdyugin & Teerikorpi 2002 and also recent results published by Xu et al. 2013). This edge defines the border between the two general longitude zones discussed above very well.

The aligned polarization within Markkanen's cloud along the local spiral (Berdyugin & Teerikorpi 2002) extends down to $b = 40°$ as part of the loop structure in Fig. 3. Markkanen's cloud is also clearly visible as a brightness enhancement in the IRAS map down to $l = 45°$ (Fig. 7).

5. Southern polar region

The region mapped around the southern Galactic pole is currently smaller than that for the NGP, but still large enough to reveal certain patterns. Figure 6 shows the SGP region in polar coordinates. This polarization map includes older data in the latitude range $-90° < b < -70°$ Berdyugin et al. 2004) and new data for $-70° < b < -60°$ obtained with the KVA telescope and the DiPol polarimeter in 2007−2009. A curve indicates the position of the inner edge of the Orion spur (the SGP is within it).

We previously (Berdyugin et al. 2004)) noted that within the latitude range closest to the pole, $-90° < b < -70°$, the polarization vectors are very well aligned in the direction corresponding to the global magnetic field $l \approx 80°$. Now we have more data up to $b = -60°$ for an extended longitude interval. The new data show relatively high and well-aligned polarizations, but the direction deviates from that observed closer to the pole area.

A clear asymmetry in the NGP and SGP maps is revealed when one compares the regions in side the Orion spur: low polarization in the NGP direction, higher and better aligned polarization in the SGP direction.

We also emphasize that our maps for $b > 30°$ *do not show* apparent signatures of the global Galactic field, which is parallel to the Galaxy plane. This becomes obvious from visual inspection of Fig. 3: the upper part is dominated by the loop-like magnetic structure and the lower part shows no structures at all. Only closer to the SGP can one see a part of the global field, but at the latitudes $b > -70°$ a different alignment appears.

6. Comparison with the IRAS map

A nonzero interstellar polarization requires elongated dust grains and a sufficiently strong and regular magnetic field aligning the grains. Therefore, it is useful to compare the optical polarization with measurements that depend in other ways on these factors, such as far-infrared IRAS maps, radio continuum polarization, soft X-ray maps, stellar reddenings, counts of galaxies, and neutral hydrogen column densities (not all of them equally suitable for high latitudes and low extinction).

For example, radio polarization (a synchrotron process) requires regular magnetic fields (and relativistic electrons – these are not directly related to dust), while the other indicators measure the amount of dust or neutral hydrogen (the latter one typically correlates with diffuse dust).

In our previous studies (Berdyugin & Teerikorpi 2002) we have already noticed the good correlation between the optical polarization map and the IRAS 100 μm map for the NGP region, as well as with the soft X-ray background (Berdyugin et al. 2000); the nearby HI gas reveals itself via the absorbtion of the soft X-ray galactic background radiation. There the most prominent polarization structure is Markkanen's cloud. It appears on

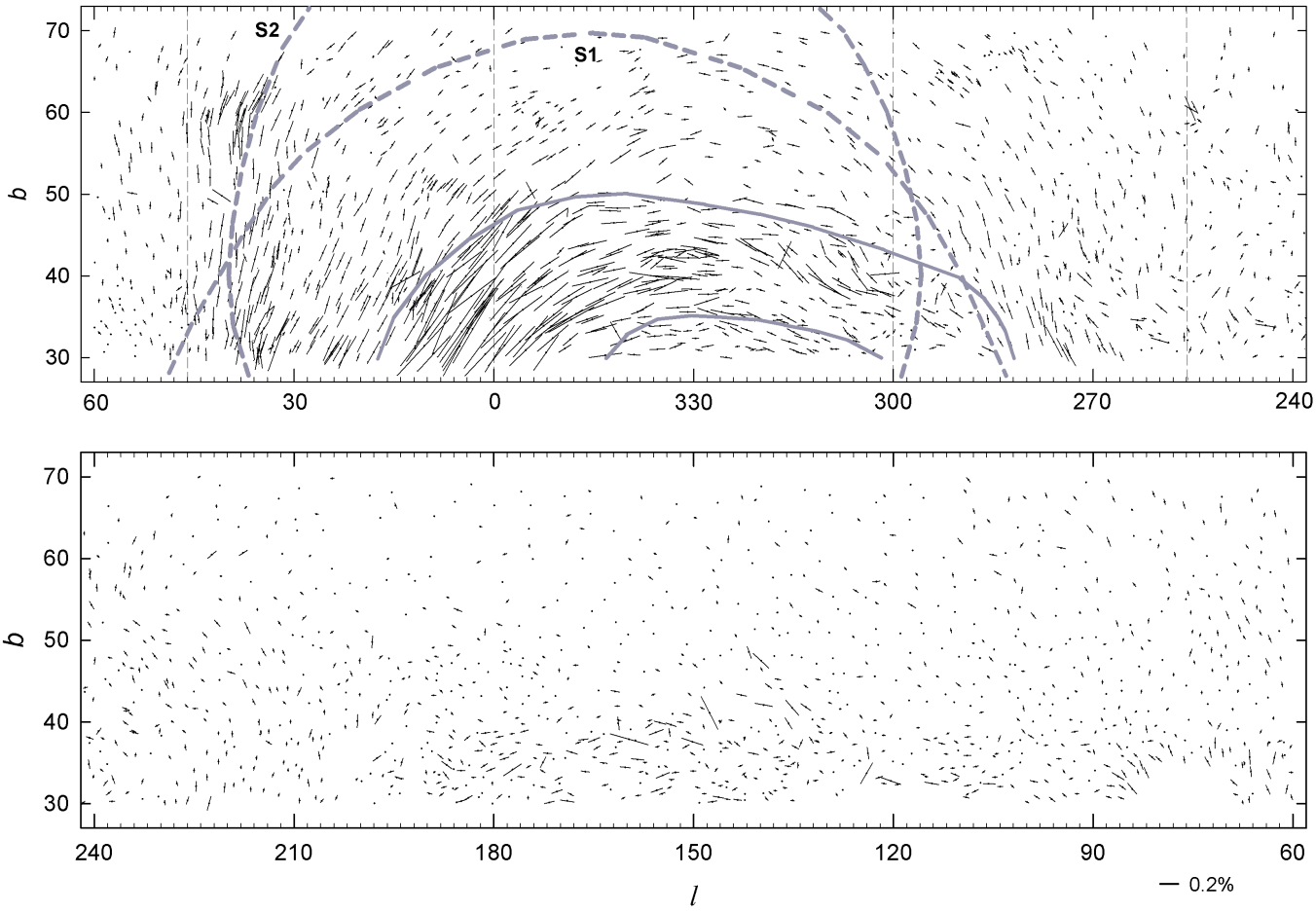

Fig. 3. Map of interstellar polarization at high northern galactic latitudes: rectangular projection. The map shows the latitude range from 30° to 70°. The length of the bar is proportional to the value of polarization P. Thin vertical dashed lines show the eastern ($255° < l < 300°$), central ($300° < l < 360°$), and western ($0° < l < 45°$) latitude zones of the magnetic loop. Thick dashed lines show the outer walls of Wolleben's S1 and S2 shells and the thick solid line shows the contour of the interaction ring between the Local Bubble and Loop I (see Sects. 8.2 and 8.3 for explanation).

the IRAS map as an area of bright elongated emission filaments aligned with the direction of the dust cloud and of the interstellar polarization inside the cloud. Figures 7 and 8 show the maps of the IRAS 100 μm emission for the NGP (up to $b = 45°$) and SGP (up to $b = -55°$) regions, respectively. One can indeed see some correlation between the areas of enhanced and well-aligned polarizations and bright emission patches for both polar zones.

Thus, interstellar polarization maps agree very well with the far-infrared data. However, we must remember that polarimetry probes the extinction (and thus the dust content) along each direction only up to a certain distance. The distance limit up to which we have a statistically significant number of measurements is about 400 pc. The IRAS maps give the estimates for the extinction from the IR emission *along the whole line of sight*. Therefore, the bright emission patches on the IRAS map that are not detected on the polarization map could be due to distant dust clouds that are not reached by our stellar polarimetry.

7. Comparison with radio polarization data

Radio polarization comes from the synchrotron process that involves magnetic field and free relativistic electrons. Although there is no direct correlation between the free electrons and the dust in the interstellar medium, a comparison of optical and radio polarization gives additional information on the interstellar magnetic field that aligns dust grains and directs relativistic electrons.

All-sky radio polarization maps at 1.4 GHz (for the northern hemisphere) and 28 Ghz (for the southern hemisphere) were compiled and published by Wolleben (2007, cf. his Fig. 1). The northern part of this map (from $l = 310°$ to $l = 50°$ and $30° < b < 80°$) is dominated by the North Polar Spur (NPS) – the brightest filament of Loop I, a large circular structure seen in the radio continuum sky. A model representing the observed large-scale polarized radio emission structures, consisting of two synchrotron-emitting shells, was proposed. According to Wolleben, one of these shells (S2) is responsible for the emission of the NPS, while the other one (S1) generates the polarized radio emission toward the Galactic poles.

The polarized radio emission map and the optical polarization map for high northern latitudes ($b > 30°$) are very well correlated. Indeed, the area of sky where high and well-aligned optical polarization is observed ($60° < l < 240°$) appears bright in radio as well. Moreover, the part of the magnetic loop seen in Fig. 3 with the highest optical polarization in the region $50° < l < 300°, 30° < b < 60°$ coincides with the area of

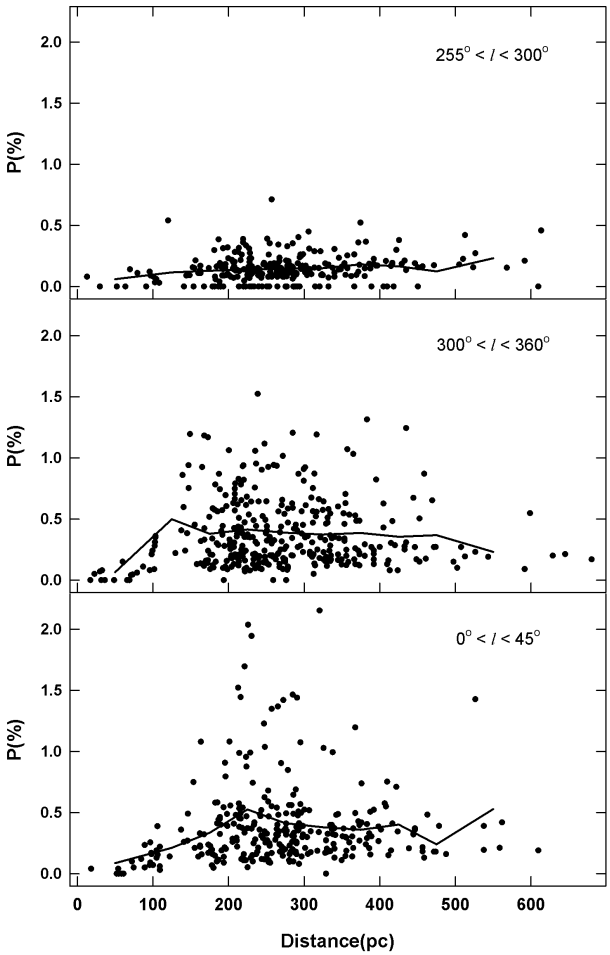

Fig. 4. Dependence of the interstellar polarization on distance in eastern, central, and western parts of the magnetic loop. Median lines are drawn for bins of 50 pc (in the distance range of 100−500 pc) and for 100 pc (up to 100 pc and beyond 500 pc). The plots show the polarizations of the stars whose error in the parallax estimation is ≤40%

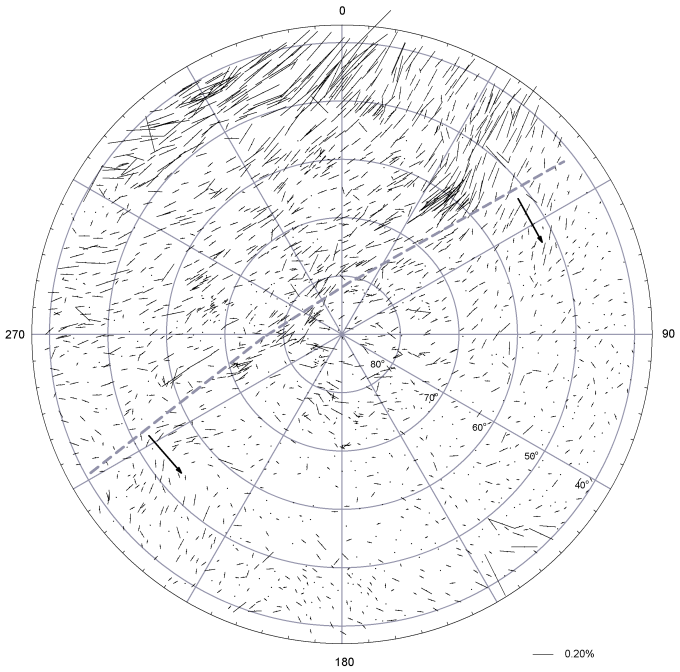

Fig. 5. NGP interstellar polarization map for the latitude range 40° < b < 90°. The gray thick line shows the approximate position of the Orion spur (the local spiral). The direction inside the spur is shown by arrows.

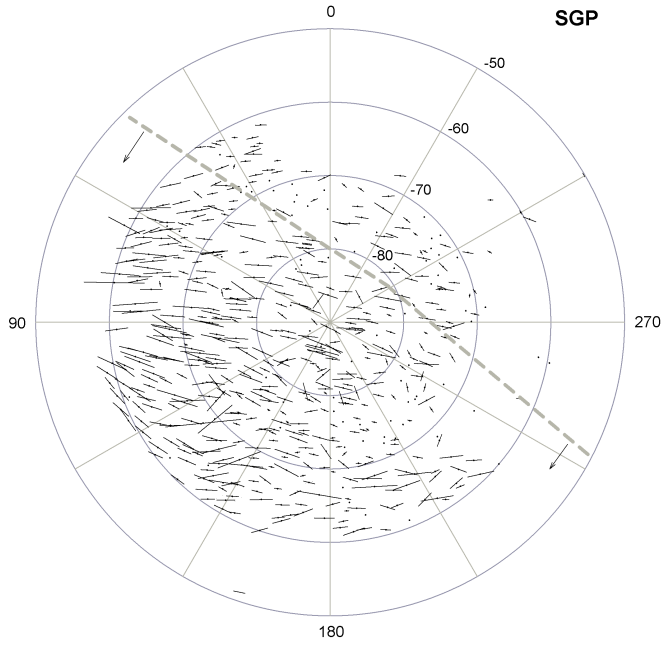

Fig. 6. SGP interstellar polarization map for the latitude range −90° < b < −60°. The gray thick line shows the approximate position of the Orion spur. The direction inside the spur is shown by arrows.

the brightest polarized emission on the radio map (cf. Fig. 1 of Wolleben 2007).

We noted above the remarkable difference between the optical polarization in the eastern and the western branch of the loop structure at high northern latitudes. Is the lower polarization in the eastern range due to little dust or a weak (irregular) Galactic magnetic field? A comparison with the IRAS 100 μm map in the latitude range 50°−60° shows that the eastern branch longitude range (255° < l < 300°) with low polarization looks bright in diffuse IR emission (hence contains a substantial amount of dust). The western range with higher polarization is less bright in far IR, but it is dominated by narrow filaments aligned in the general direction of polarization (a part of Markkanen's cloud).

In comparison, the radio polarization map of Wolleben (2007) shows much more weakly polarized emission in the eastern branch than in the western part. Because radio polarization arises from synchrotron process, this suggests that here the magnetic field (or its relevant component) is weaker. This may be an example of the interplay between the amount of dust, its alignment, and the polarization: low optical polarization does not necessarily imply little dust (i.e. $A_V \geq P_V/3.0$). Note that the low polarization in the eastern branch is nevertheless aligned very well, which suggests a regular direction of the Galactic magnetic field in this region. We discuss Wolleben's model in more detail in Sect. 8.2.

8. Interpreting polarization patterns

The most striking feature in our maps is, of course, the large northern magnetic loop and the related strong polarization alignments seen in Fig. 3.

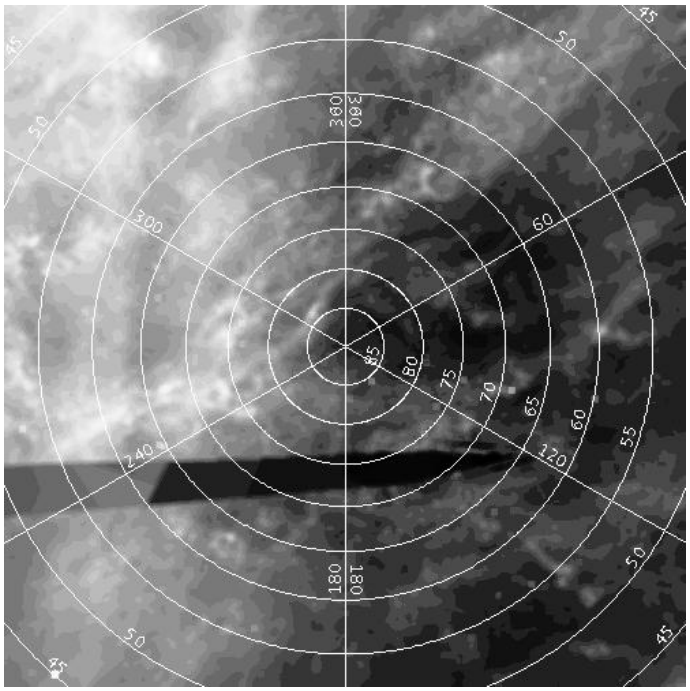

Fig. 7. IRAS 100 μm map of the NGP area down to $b = 45°$. The orientation corresponds to that of the polarization map of Fig. 5.

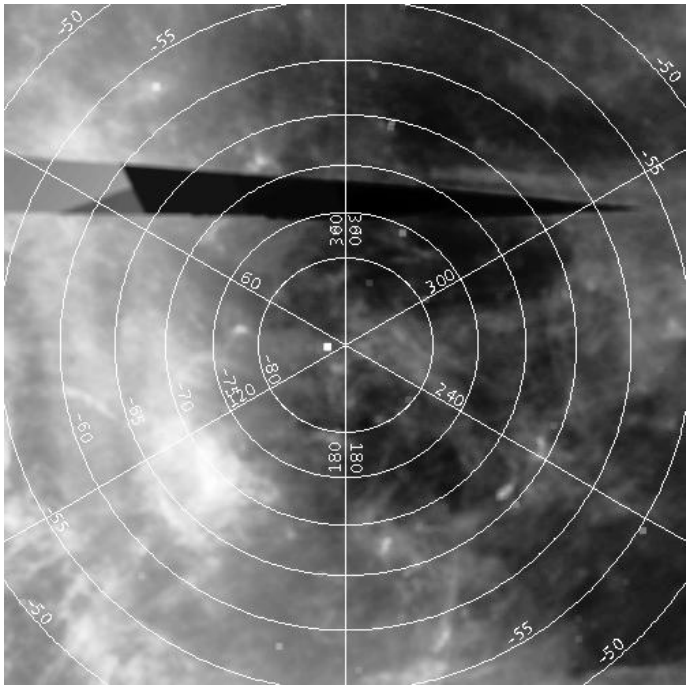

Fig. 8. IRAS 100 μm map of the SGP area down to $b = -55°$. The orientation corresponds to that of the polarization map of Fig. 6.

8.1. Weaver's superbublle

After the discovery by Mathewson & Ford (1970), the loop was identified as a polarized synchrotron radiation structure by Berkhuijsen (1971) and Ellis & Axon (1978). Weaver (1979) explained it as an expanding gas- and dust shell resulting from a supernova explosion several tens of parsecs from the Sun a few million years ago. Such superbubbles cause detours in the local Galactic magnetic fields. The nearest one, the so-called local superbubble or Loop I is regarded as responsible for the well-known feature in the polarized radio emission (the North Polar Spur) and for the optical polarization loop here discussed.

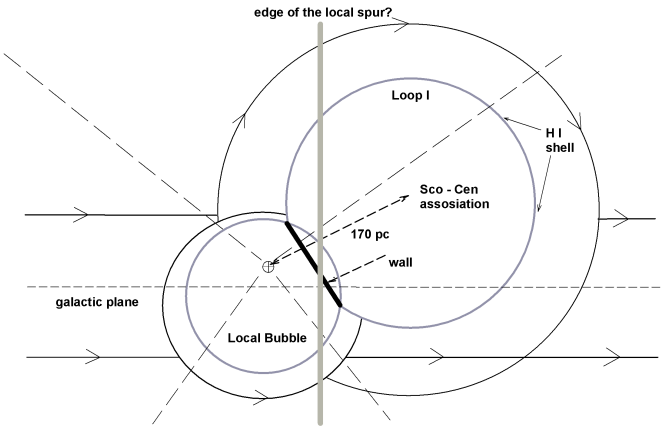

Fig. 9. Possible sketch of our local Galactic environment with the deformed magnetic field (adopted from Vallée 2004). The areas covered by our observations are within the cones shown with the dashed lines. The approximate position of the edge of the Local spur is drawn with the thick vertical line.

The common view is that this shell is centered at $l = 330°, b = 17.5°$ and thus our map depicts the upper horizontal slice of this magnetic loop. Figure 9 shows a sketch of the local Galactic magnetic field as adopted from Vallée (2004). According to this picture, the Sun is located inside the local hole (Local bubble) and about 20 pc above the galactic plane. We have added dashed lines that roughly show the polar areas covered by our polarization maps.

The HI shell around Loop I and the wall between the Local bubble and the Loop I superbubble is apparent in the map based on the soft X-ray data obtained by ROSAT (e.g. Egger & Aschenbach 1995). From polarimetry of nearby stars, Tinbergen (1982) and Leroy (1999) found virtually no polarization up to about 50 pc from the Sun (the local void). Traces of measurable polarization appear at a distance ≈70 pc, which was interpreted as being due to the wall of dust in the shell of the Loop I superbubble (Tinbergen 1982).

Our polarization data give no apparent evidence for wall-like structures in the radial distribution of the dust in the direction of the Loop I superbubble. As seen from Fig. 4, in the northern high-latitude part of the sky that encompasses Loop I, polarization grows linearly with distance, reaching its average maximum at about 200−250 pc. Moreover, the values of polarization in the eastern and central part of the loop within the distance range 200−400 pc show a large scatter, from 0.0 to 1.5%. This argues strongly against a simple regular structure in the radial distribution of dust, such as a wall and a void. Hence, the true picture may somewhat differ from the sketch in Fig. 9. In fact, a more complex model comprising two local superbubbles has recently been proposed.

8.2. Wolleben's two-bubble model

Wolleben (2007) modeled the polarized emission in the northern radio sky using two (instead of one) synchrotron emitting spherical shells S1 and S2. The Sun is located within S1, between its inner and outer surfaces. The centers of the shells are at $l \approx 346°, b \approx 3°$ (S1) and $l \approx 347°, b \approx 37°$ (S2), in the general direction of the I and IV Galactic quadrants. This geometry

explains the location of the enhanced alignments (in radio) in these directions and the weak polarized emission at high latitudes around $l \approx 180°$ (cf. Figs. 3 and 4 in Wolleben 2007).

Wolleben noted that the diffuse high-latitude polarized radio emission is produced by S1 (the Sun is inside this shell), while S2 produces the polarized emission of the North Polar Spur. The new loop, identified by Wolleben, is seen at intermediate latitudes where the perpendicular B component of S2 is longest.

We have drawn the approximate position of the outer walls of Wolleben's shells S1 and S2 in our polarization map in Fig. 3 with the thick dashed line. Obviously, because the S1 is very close in position and similar in shape to the well-known Loop I, one can clearly see the structure resembling it on the map. But can we see any signatures of S2 and the new loop? S2 should be visible best, from the polarization directions, at the longitude ranges $l = 60°-30°$ and $l = 310°-280°$. In the latitude range between $30° < b < 60°$ we expect to see the directions of interstellar polarization aligned nearly perpendicular to the galactic plane. Indeed, this is the case for the part of the sky where the western wall of S2 is to be located. As one can see in Fig. 3, in the coordinate range $l \approx 55°-35°, b \approx 30°-50°$, the polarization vectors follow the expected direction of the western wall of S2 shell very well. However, this is not the case for the eastern part: there is no apparent co-alignment of the directions of polarization along the wall of S2, but the alignment along the wall of S1 (or Loop I) is clearly visible.

Of course, if we adopt Wolleben's model, we must accept that the observed direction of the optical polarization is a result of a complex interplay between the directions of the magnetic fields in S1 and S2 (depending on the distance) and the radial distribution of the dust. In principle, looking at the geometry of S1 and S2, and the location of the Sun (cf. Fig. 3 in Wolleben 2007), one may expect that in the eastern direction ($l \approx 300°$) the dust grain alignment must be stronger influenced by the magnetic field in shell S1. This may account for the observed general directions of polarization in the eastern longitude range.

The two-shell model may also explain the observed difference in the magnitude of the optical polarization in the eastern and western branches of Loop I: in the direction toward $l \approx 50°-0°$ the line of sight travels mostly *inside two closely adjoining walls* of the S1 and S2 shells extending to the high latitude area at the distance of more than ≈150 pc and (presumably) filled with dust. In the eastern directions $l \approx 340°-290°$ the line of sight extends mostly through the *voids* inside the shells (cf. Figs. 3 and 4 in Wolleben 2007).

The signature of the new loop identified by Wolleben, should be visible best at southern high latitudes, in the area $l \approx 300°-60°, b \approx -30°-70°$. Because our southern high-latitude polarization map covers only a small part of this area, new measurements using a telescope located in the southern hemisphere are needed to verify this prediction.

8.3. Interaction zone between the Local bubble and Loop I

As we mentioned above, a ring-like wall between the Local bubble and the Loop I superbubble (cf. Fig. 9) was proposed by Egger & Aschenbach (1995). The distance to this interaction region is somewhat uncertain. A recent analysis of the $E(b-y)$ data made by Reis & Corradi (2008) suggests that the western (left) side of the wall is at the distance of 110 ± 20 pc, while the eastern (right) side cannot be seen clearly before 280 ± 50 pc.

Recently, Santos et al. (2011) have mapped the optical polarization within this interaction zone by observing about 900 stars up to the distance of ≈250 pc. They measured the polarizations within the ring comprising this interaction area (located between $270° < l < 40°, -40° < b < 50°$ with the center at $l \approx 330°, b \approx 0°$, cf. Fig. 5 in their paper). For the comparison with our study, the measurements made by Santos et al. (2011) for the stars in the upper part of the ring ($30 < b < 50$) are the most interesting.

According to their results, this structure appears to be "highly twisted and fragmented, showing very discrepant distances along the annular region: ≈100 pc on the left side and 250 pc on the right side". They also found that the directions of polarization behave differently at different sides of the structure: "running parallel to the ring contour on the left side and showing no relation to its direction on the right side".

We have plotted the uppermost part of the contour of the interaction ring in our polarization map in Fig. 3. Our observations were made mostly for the stars at distances *larger* than 250 pc and it is interesting to compare our map with the map made by Santos et al. (2011) for more nearby stars. We also have a good coverage of the sky around the upper part of the interaction ring.

In the area of $l = 320°-280°, b = 30°-50°$ in Fig. 5 of Santos et al. (2011), one can see only low and more or less randomly directed polarization. Our map shows slightly different picture: the polarization values are indeed lower than in the western part of the ring, but the polarization directions, nevertheless, appear to be aligned along the ring contour. A similar alignment is also visible just outside of the ring borders.

Do our results suggest that the interaction wall between the Local bubble and Loop I at the eastern side should be sought at distances larger than 250 pc? Although our data may give this impression, we note that they refer to the uppermost part of the interaction ring, where the polarization picture for distant stars may be strongly influenced by the magnetic field in the Loop I itself. In fact, it is very difficult to distinguish clearly between two (or even three) structures that are superimposed here, namely: 1) the upper part of the interaction ring; 2) Loop I; or 3) Wolleben's shells S1 and S2. Structures 1) and 2) imply more or less similar polarization directions. However, the detailed picture at the eastern side of Loop I as seen from Fig. 3 appears to be even more complex.

9. Conclusions

The new interstellar polarization maps, which use ≈2400 new stars with polarization measured by us in addition to the older data, give wider and higher resolution views around the Galactic poles than previous maps. The main striking patterns are the significant asymmetries in the polarization, one in the northern sky directly across the local spiral and the second between the northern and southern Galactic hemispheres. We confirmed that the average value of interstellar polarization at high southern latitudes is significantly higher than at high northern latitudes within the local spiral. Markkanen's cloud as part of the aligned magnetic field structure that extends to lower latitudes is clearly seen as the giant loop centered around $l = 330°$.

It follows from our new extended data set that the interstellar polarization maps agree very well with the existing far-infrared IRAS data.

Our detailed map of the interstellar polarization at the nothern high galactic latitudes shows no signature of the global Galactic magnetic field, which is parallel to the plane of the Galaxy (cf. Fig. 3). It appears that for the latitudes $b > 30°$ and distances $d < 400$ pc the geometry of the Galactic magnetic field around the Sun is entirely dominated by the local structures, whose directions deviate from the geometry of the global field.

When comparing our optical polarization map with the proposed models using local dust- and gas shells (Weaver's Loop I superbubble, Wolleben's two-bubble model, the interaction between the Local Bubble and the Loop I superbubble), we can emphasize the following points:

- Our polarization data do not reveal wall-void structures in the distribution of the dust toward the Loop I superbubble.
- We see a clear signature of the western side of Wolleben's S2 shell (at $35 < l < 55$), while in the eastern part there is no alignment of the polarization directions along the suggested wall of S2, though the alignment along S1 is visible.
- The different polarizations in the eastern (lower P) and western (higher P) branches of Loop I may be caused by a weaker effective magnetic field in the eastern part, because the radio polarization is there also weak, while the diffuse IRAS emission is bright. This illustrates the fact that low optical polarization does not necessarily imply little dust. It should be also noted that according to Wolleben's S1 + S2 model, our lines of sight in the eastern and western parts intersect these two shells in different ways.
- In the upper eastern part of the suggested interaction zone between the Local Bubble and the Loop I superbubble our data show substantial polarizations aligned along the ring contour. The low and randomly directed polarizations as measured by Santos et al. (2011) in this region may reflect the shorter distances (<250 pc) in their sample, compared with our sample. However, we are not inclined to interpret our results as firm evidence for the interaction wall in this direction at the distances >250 pc. It appears that the real picture of the distribution of dust here is more complex and cannot be clearly revealed with the available data, especially when considering the uncertainties in stellar distances.

Acknowledgements. Part of this work was supported by the German *Deutsche Forschungsgemeinschaft, DFG* project number Ts 17/2–1.

References

Appenzeller, I. 1968, ApJ, 151, 907
Appenzeller, I. 1975, A&A, 38, 313
Berdyugin, A., & Teerikorpi, P. 2002, A&A, 384, 1050
Berdyugin, A., Teerikorpi, P., & Haikala, L. 2000, A&A, 358, 717
Berdyugin, A., Teerikorpi, P., Haikala, L., et al. 2001, A&A, 372, 276
Berdyugin, A., Piirola, V., & Teerikorpi, P. 2004, A&A, 424, 873
Berkhuijsen, E. M. 1971, A&A, 14, 359
Egger, R. J., & Aschenbach, B. 1995, A&A, 294, L25
Ellis, R. S., & Axon, D. J. 1978, Ap&SS, 54, 425
Korhonen, T., & Reiz, A. 1986, A&AS, 64, 487
Leroy, J. L. 1999, A&A, 346, 955
Markkanen, T. 1979, A&A, 74, 201
Mathewson, D. S., & Ford, V. L. 1970, MmRAS, 74, 139
Piirola, V., Berdyugin, A., Mikkola, S., & Coyne, G. V. 2005, ApJ, 632, 576
Reis, W., & Corradi, W. 2008, A&A, 486, 471
Santos, F. P., Corradi, W., & Reis, W. 2011, ApJ, 728, 104
Shroder, R. 1976, A&AS, 23, 125
Tinbergen, J. 1982, A&A, 105, 53
Vallée, J. P. 2004, New Astron. Rev., 48, 763
Weaver, H. 1979, 84, 295
Wolleben, M. 2007, ApJ, 664, 349
Xu, Y., Li, J. J., Reid, M. J., et al. 2013, ApJ, 769, 15